Electronic Supplementary Material (ESI) for ChemComm.

High-contrast polymorphic difluoroboron luminogen with efficient RTP and TADF emission in solid states

Xin Wang[a,b], Xiaofu Wu[a], Tong Wang[a,b], Yuliang Wu[a,b], Haiyang Shu[a,b], Zhiqiang Cheng[a,b], Lei Zhao[a], Hongkun Tian[a,b], Hui Tong*[a,b], Lixiang Wang*[a,b]

[a] X. Wang, Dr. X. Wu, T. Wang, Y. Wu, H. Shu, Z. Cheng, Dr. L. Zhao, Prof. H. Tian, Prof. H. Tong, Prof. L, Wang
State Key Laboratory of Polymer Physics and Chemistry
Changchun Institute of Applied Chemistry
Chinese Academy of Sciences, Changchun 130022 (P. R. China) E-mail: chemtonghui@ciac.ac.cn, lixiang@ciac.ac.cn

[b] X. Wang, Dr. X. Wu, T. Wang, Y. Wu, H. Shu, Z. Cheng, Dr. L. Zhao, Prof. H. Tian, Prof. H. Tong, Prof. L, Wang
University of Science and Technology of China
Hefei 230026 (P. R. China)

Table of Contents

1. Experimental Details

1.1. Materials and Reagents. 4-bromobenzaldehyde, pyridin-2-amine, 9,9-dimethyl-9,10-dihydroacridine (DMAC)， boron trifluoride diethyl etherate ($BF_3 \cdot OEt_2$) and Lawesson reagent were purchased from energy chemical. All solvents were purified and distilled using standard procedures before use. All others were analytical reagents and were used without further purification.

1.2. Physical Measurements and Instrumentation. ^1H NMR, ^{13}C NMR and $^{19}F\{1H\}$ NMR spectroscopy were recorded at 500 MHz (Bruker AV) with TMS as the internal standard. All chemical shifts are given in ppm and all coupling constants (*J* values) are reported in Hertz (Hz). High-resolution mass spectra were obtained by using LTQ Orbitrap Velos Pro. The UV-vis absorption spectra were recorded on a Perkin-Elmer Lambda 35 UV/Vis spectrometer.The steady-state emission spectra, transient PL spectra and time-resolved PL spectra were all detected on an Edinburgh fluorescence spectrometer (FLS-980). The absolute luminescence quantum yields were measured on an integrating sphere (Hamamatsu Photonics C9920-2). The single crystal X-ray diffraction experiments were carried out using a Bruker Smart APEX diffractometer with CCD detector and graphite monochromator, Mo Kα radiation (λ =0.71073 Å). The intensity data were recorded with ω scan mode. Lorentz, polarization factors were made for the intensity data and absorption corrections were performed using SADABS program. Thermal gravimetric analysis (TGA) and differential scanning calorimetry (DSC) were performed with a Perkin-Elmer-TGA 7 and a PerkinElmer-DSC 7 in N_2 at a heating rate of 10 °C/min.

1.3. Preparation of G-, Y- and R-crystals. Three polymorphs of this compound were prepared by solution self-assembly method in different solution. Briefly, dissolve DMAC-PSBF2 (25 mg) in DCM (2.5 ml), then add n-hexane (5.0 ml) or methanol (5.0 ml). Through slow evaporation of the DCM, the G- and Y-Crystals were obtained, respectively. G-Crystal was a green-yellow needle. Y-Crystal exhibited smaller orange slab-like crystal. Surprisingly, the platelet-like red crystal R-Crystal was also gained, through evaporation of the mixture solution of DMAC-PSBF2 (25 mg) in toluene (2.5 ml) and n-hexane (5.0 ml). Through repeating the single crystal growth procedures, we have finally got 49, 66, and 83 mg samples of G-, Y- and R-Crystal, respectively.

2. Synthesis and characterization

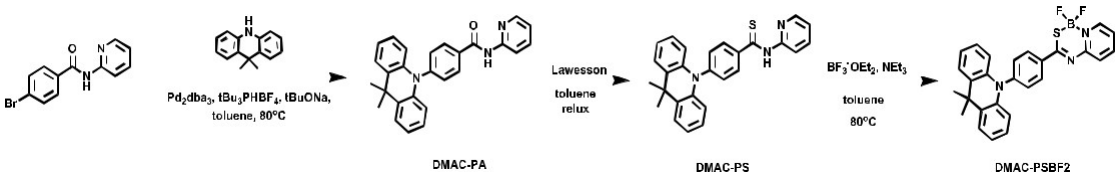

Scheme S1. The synthetic routes of compound DMAC-PSBF2.

4-bromo-N-(pyridin-2-yl)benzamide was synthesized according to the previously reported method[1].

a) Synthesis of 4-(9,9-dimethylacridin-10(9H)-yl)-N-(pyridin-2-yl)benzamide (DMAC-PA) : A mixture of 9,9-dimethyl-9,10-dihydroacridine (DMAC, 753 mg, 3.6 mmol), 4-bromo-N-(pyridin-2-yl)benzamide (1.0 g, 3.6 mmol), Pd_2dba_3 (285.0 mg, 0.3 mmol), t-Bu_3PHBF_4 (72.6 mg, 1.44 mmol), t-BuONa (1.0 g, 10.8 mmol) and anhydrous toluene (50 ml) was added into a two-neck round bottom flask with a tempeture of 120 ^oC overnight under an argon atmosphere. After cooling to room temperature, the mixture was extracted with deionized water and dichloromethane, and dried over anhydrous Na_2SO_4. After removal of the solvent under reduced pressure, the crude product was purified by column chromatography on silica gel using ethyl acetate /petroleum ether (1:2) as the eluent to afford a yellow solid (700 mg, 48%). ^1H NMR (500 MHz, $CDCl_3$) δ = 8.96 (s, 1H), 8.46 (d, *J*=8.4 Hz, 1H), 8.32–8.29 (m, 1H), 8.20 (d, *J*=8.4 Hz, 2H), 7.82 (td, *J*=8.6 Hz, 1.8 Hz, 1H), 7.53–7.45 (m, 4H), 7.15–7.10 (m, 1H), 7.02–6.93 (m, 4H), 6.28 (dd, *J*=7.9 Hz, 1.4 Hz, 2H), 1.69 (s, 6H). ^{13}C NMR (126 MHz, $CDCl_3$) δ = 165.12, 151.45, 147.64, 145.25, 140.44, 138.83, 133.89, 131.63, 130.51, 129.98, 126.43, 125.36, 121.08, 120.12, 114.39, 114.20, 36.05, 31.13.

b) Synthesis of 4-(9,9-dimethylacridin-10(9H)-yl)-N-(pyridin-2-yl)benzothioamide (DMAC-PS) : A solution of the amide DMAC-PA (1.3 g, 3.0 mmol) in 30 mL of dry toluene was treated with 808 mg (2.0 mmol) of Lawesson reagent, and homogeneous solution was heated under reflux in the atmosphere of argon for 3 h. The progress of the reaction was monitored by TLC on plates coated with neutral alumina using ethyl acetate. When the reaction was finished, the solvent was evaporated, and the crude mixture was separated by column chromatography on neutral alumina using a 1:1 mixture of ethyl acetate and petroleum. A yellow colored fraction was isolated and identified as the required thioamide DMAC-PS (821 mg, 65%). ^1H NMR (500 MHz, DMSO) δ = 12.32 (s, 1H), 8.54 (s, 1H), 8.40 (s, 1H), 8.10 (s, 2H), 7.95 (t, *J* = 7.7 Hz, 1H), 7.51 (d, *J* = 7.7 Hz, 2H), 7.44 (d, *J* = 7.8 Hz, 2H), 7.39 – 7.30 (m, 1H), 7.01 (t, *J* = 7.6 Hz, 2H), 6.93 (t, *J* = 7.4 Hz, 2H), 6.23 (d, *J* = 8.2 Hz, 2H), 1.63 (s, 6H).^{13}C NMR (126 MHz, DMSO) δ = 153.16, 149.04, 143.47, 142.36, 140.49, 138.34, 130.88, 130.86, 130.33, 126.96, 126.01, 122.49, 121.27, 118.94, 114.22, 36.07, 31.75.

c) Synthesis of 3-(4-(9,9-dimethylacridin-10(9H)-yl)phenyl)-1,1-difluoro-1H-1l4,9l4-pyrido[1,2-c] [1,3,5,2] thiadiazaborinine (DMAC-PSBF2) : A mixture of DMAC-PS (1.6 g, 3.8 mmol), anhydrous

triethylamine (7.6 ml, 53 mmol), and 180 mL of anhydrous dichloromethane stirred at room temperature and then boron trifluoride ethyl ether complex (11 ml, 91 mmol) was added dropwise. The reaction mixture was stirred at room temperature overnight. Then the mixture was extracted with deionized water and dichloromethane. The organic layer was dried with anhydrous Na_2SO_4, filtered, and the filtrate was concentrated under reduced pressure. The residue was purified through column chromatography on silica gel using petroleum /acetyl acetate (3:1) as eluent to afford a yellow solid (410 mg, 23%). ^{1}H NMR (500 MHz, $CDCl_3$) δ = 8.66 (d, *J* = 5.6 Hz, 1H), 8.60 (d, *J* = 8.5 Hz, 2H), 8.25–8.18 (m, 1H), 7.85 (d, *J* = 8.3 Hz, 1H), 7.59–7.54 (m, 1H), 7.52–7.44 (m, 4H), 7.02–6.94 (m, 4H), 6.37 (dd, *J* = 7.9, 1.3 Hz, 2H), 1.70 (s, 6H). ^{13}C NMR (126 MHz, $CDCl_3$)

δ = 178.55, 154.64, 145.97, 143.34, 140.47, 138.80, 137.14, 137.10, 131.50, 130.70, 126.65, 126.43, 125.32, 121.84, 121.10, 114.54, 36.09, 31.12. ^{19}F NMR (471 MHz, $CDCl_3$) δ = -133.30. HRMS (MALDI) m/z calcd: 469.2 $[M]^+$; found: 469.2 $[M]^+$.

3. Photophysical properties

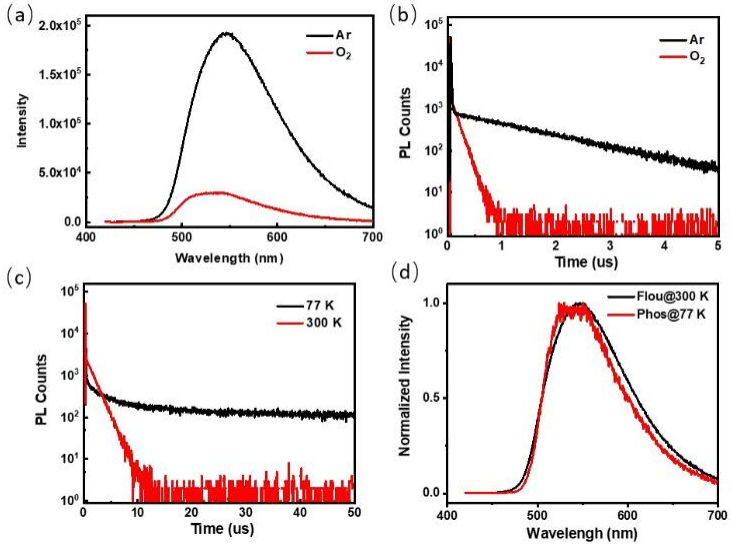

Figure S1. Steady-state (a) and transient PL decay spectra (b) of DMAC-PSBF2 in n-hexane solution (1×10^{-6} M) at Ar or O_2 condition. Transient PL decay (c), steady-state and delayed PL spectra (d) of DMAC-PSBF2 in n-hexane solution (1×10^{-6} M) at 77 K and 300 K.

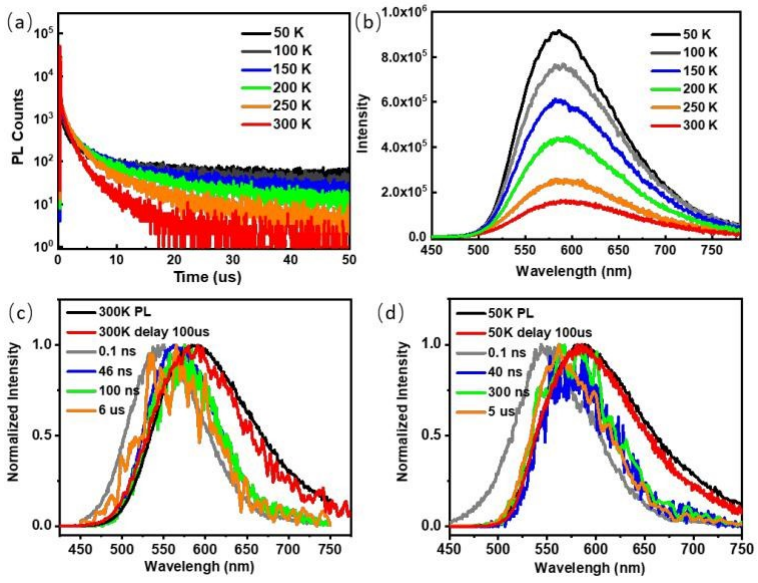

Figure S2. Temperature-dependent transient PL decay (a), steady-state PL spectra (b) , time-resolved PL spectra at 300 K (c) and 50 K (d) of DMAC-PSBF2 doped in PMMA (1 wt%).

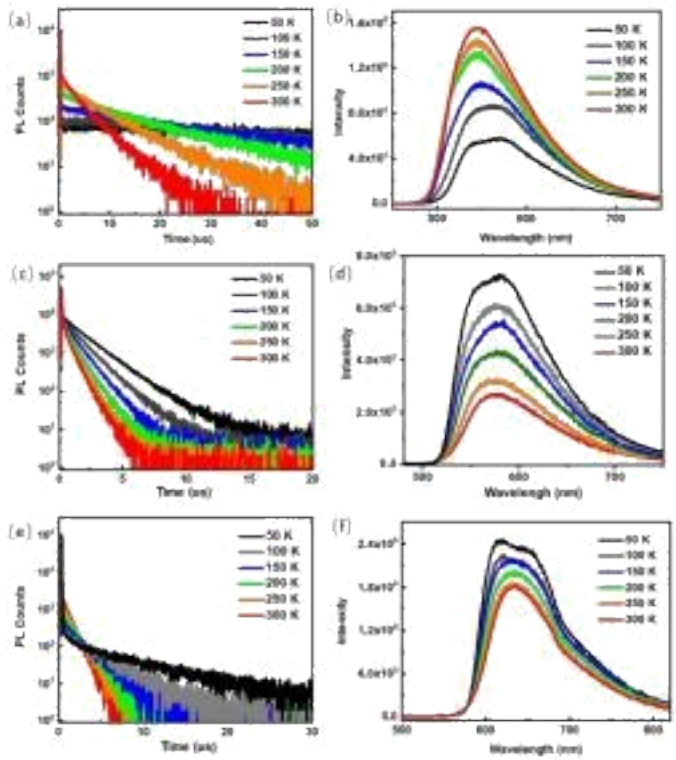

Figure S3. Temperature-dependent transient PL decay (a, c, e) and steady-state PL spectra (b, d, f) of G-Crystal (a, b), Y-Crystal (c, d) and R-Crystal (e, f), respectively.

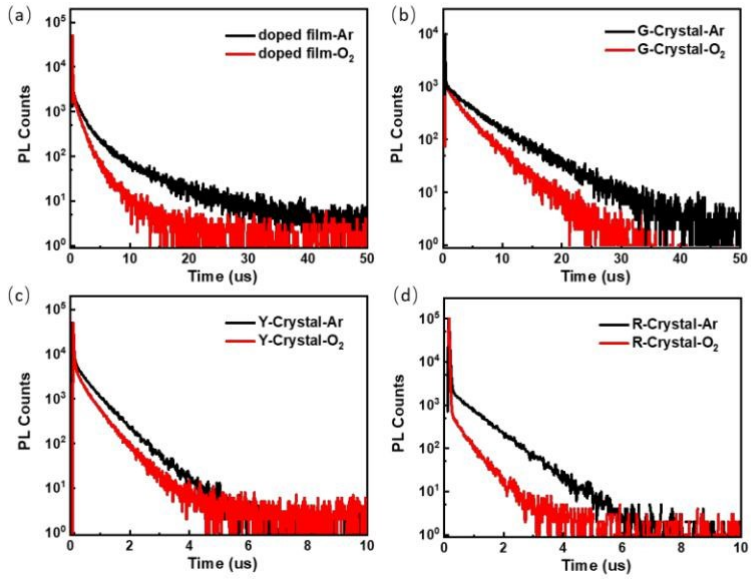

Figure S4. Transient PL decay spectra of DMAC-PSBF2 in doped film (1 wt% doped in PMMA) (a), G-Crystal (b), Y-Crystal (c) and R-Crystal (d) at Ar or O_2 condition.

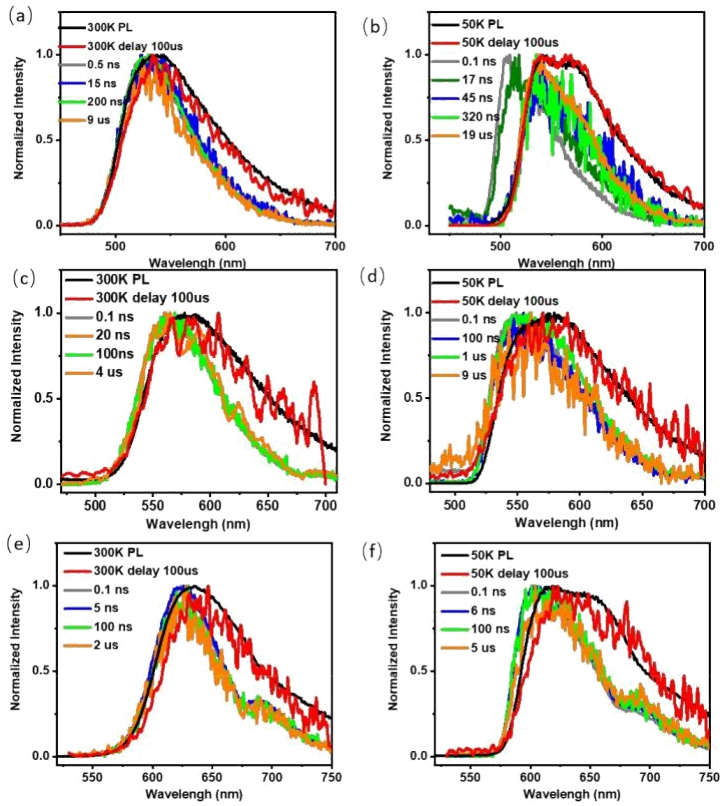

Figure S5. Time-resolved PL spectra at 300 K (a, c, e) and 50 K (b, d, f) of G-Crystal (a, b), Y-Crystal (c, d) and R-Crystal (e, f), respectively.

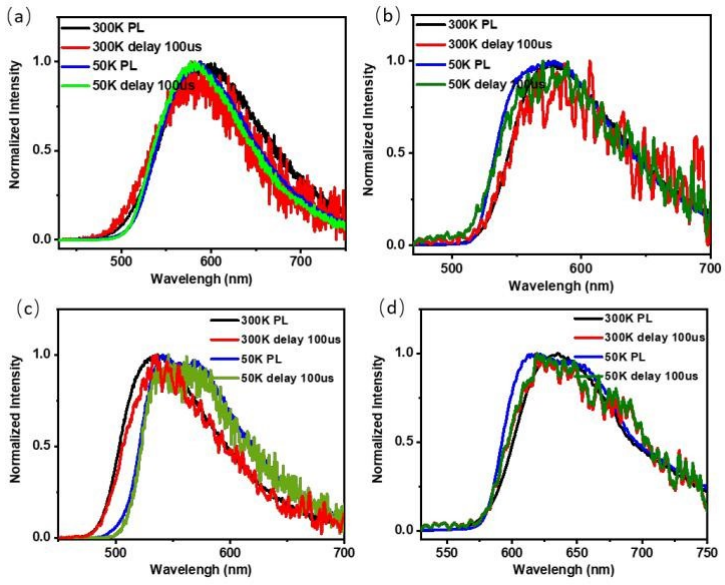

Figure S6. Steady-state and delayed PL spectra of of DMAC-PSBF2 doped in PMMA (1 wt%) (a), Y-Crystal (b), G-Crystal (c) and R-Crystal (d) at 300 K and 50 K, respectively.

4. Single crystal analysis

The crystal structure was determined using the SHELXTL program and refined using full matrix least squares. All non-hydrogen atoms were assigned with anisotropic displacement parameters, whereas hydrogen atoms were placed at calculated positions theoretically and included in the final cycles of refinement in a riding model along with the attached carbons. The obtained crystallographic parameters of G-Crystal, Y-Crystal and R-Crystal were summarized in Table S1 and CCDC reference numbers are 2166936, 2166937 and 2166938. The wR2 value of G- and Y-Crystal can not regulate to a smaller level after many attempts.

Table S1. Crystallographic date for single crystals of G-Crystal, Y-Crystal and R-Crystal.

Identification code	G-Crystal	Y-Crystal	R-Crystal
CCDC No	2166936	2166937	2166938
Empirical formula	$C_{27}H_{22}BF_2N_3S$	$C_{27}H_{22}BF_2N_3S$	$C_{27}H_{22}BF_2N_3S$
Formula weight	469.34	469.34	469.34
Temperature/K	173	293(2)	250(2)
Crystal system	triclinic	monoclinic	orthorhombic
Space group	P-1	P21/c	Pbca
a/Å	7.9268(10)	13.7071(6)	7.1491(18)
b/Å	9.2977(14)	17.6856(7)	13.136(4)
c/Å	30.925(5)	9.0346(4)	46.626(14)
α/°	91.670(5)	90	90
β/°	90.466(4)	98.4820(10)	90
γ/°	97.090(4)	90	90
Volume/$Å^3$	2260.7(6)	2166.20(16)	4566(2)
Z	4	4	8
ρ_{calc} g/cm^3	1.379	1.439	1.365
μ/mm^{-1}	0.181	0.189	0.180
2Θ range for data collection/°	3.954 to 58.422	3.004 to 54.242	5.94 to 58.46
Reflections collected	35864	31748	25645
Independent reflections	11921 [Rint = 0.0675, Rsigma = 0.0733]	4652 [Rint = 0.0579, Rsigma = 0.0365]	6140 [Rint = 0.0458, Rsigma = 0.0438]
F^2	1.198	1.089	1.028
Index ranges	-9 ≤ h ≤ 10 -12 ≤ k ≤ 12 -42 ≤ l ≤ 42	-17 ≤ h ≤ 17 -21 ≤ k ≤ 22 -11 ≤ l ≤ 11	-9 ≤ h ≤ 8 -18 ≤ k ≤ 17 -66 ≤ l ≤ 63
R_1[I > 2σ(I)] [a]	0.1165	0.0509	0.0476
wR_2[I > 2σ(I)] [b]	0.3172	0.1644	0.1166
R_1(all data)	0.1382	0.0706	0.0753
wR_2(all data)	0.3383	0.2425	0.1369

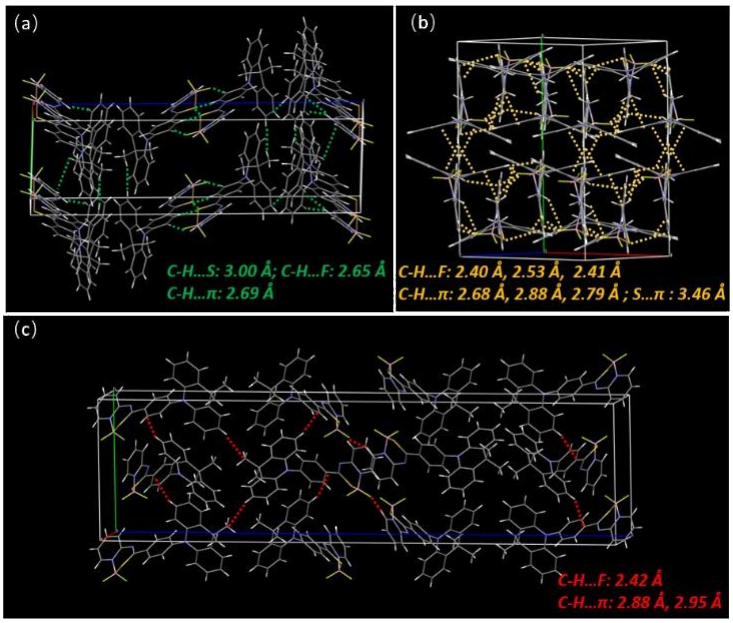

Figure S7. The crystal cell and related intermolecular interaction of G-Crystal (a), Y-Crystal (b) and R-Crystal (c).

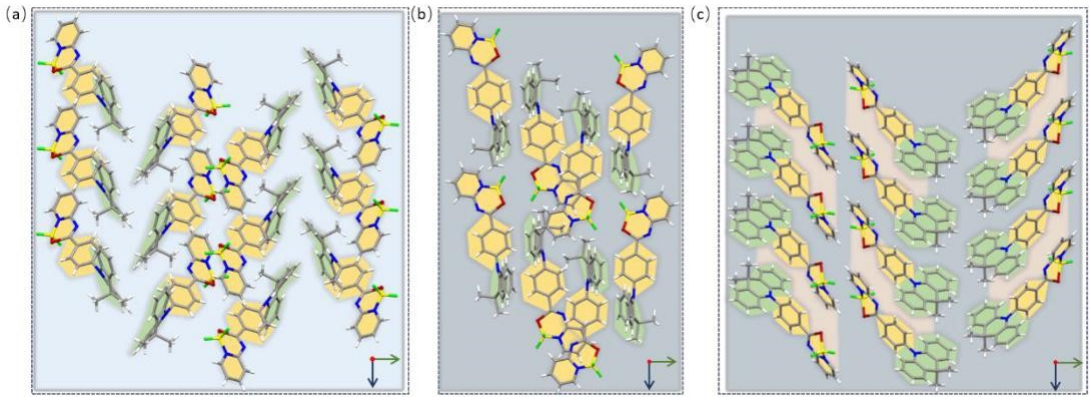

Figure S8.The molecular packing mode of G-Crystal (a), Y-Crystal (b) and R-Crystal (c).

The different conformations of G-Crystal:

G-Crystal belongs to the triclinic space group P-1, there exist two different molecular conformations: G1 and G2. The molecular structure of G1 and G2 are quite similar, the bond lengths are almost equal as can be seen from Table S2. The only difference between G1 and G2 is that the Sulfur atom are twisted in opposite direction in the coordinated ring plane (Figure S9).

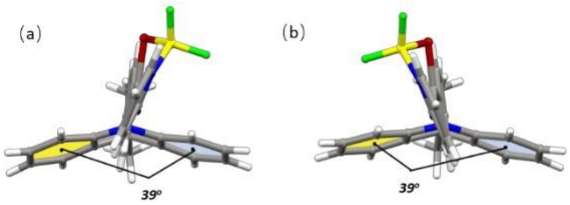

Figure S9. Molecular structure of G1 (a) and G2 (b) monomer.

Table S2. Bond length of the coordinated cycle of different molecular conformations

	monomer	1-B… F (Å)	2-B… S (Å)	3-B… N (Å)	4-S… C (Å)	5-N… C (Å)	6-C… N (Å)	7-C… N (Å)
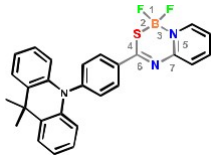	G1	1.37	1.92	1.58	1.75	1.36	1.30	1.38
	G2	1.38	1.91	1.58	1.74	1.35	1.30	1.38
	Y	1.37	1.90	1.56	1.73	1.34	1.29	1.36
	R	1.37	1.93	1.57	1.75	1.36	1.29	1.38

5. Theoretical calculations

All the density functional theory (DFT) and time-dependent DFT (TD-DFT) calculations were performed with the Gaussian 09 program suite. The ground-state (S_0) geometries of DMAC-PSBF2 were optimized by M06-2x/TZVP level or obtained in the crystals. TD-DFT calculations at M06-2x/TZVP level were carried out to investigate the excited state properties of these conformations. We also performed Natural Transition Orbital (NTO) analysis to estimate the characterization of the excited states as local excited (LE) or charge transfer (CT) using Multiwfn 3.7 [2]. The orbital coupling constants (SOC) were determined at the M06-2x/TZVP level on ORCA 4.1.0 [3], and they were calculated using the structures in different crystals.

5.1. The calculation data of monomers and dimers in three crystals

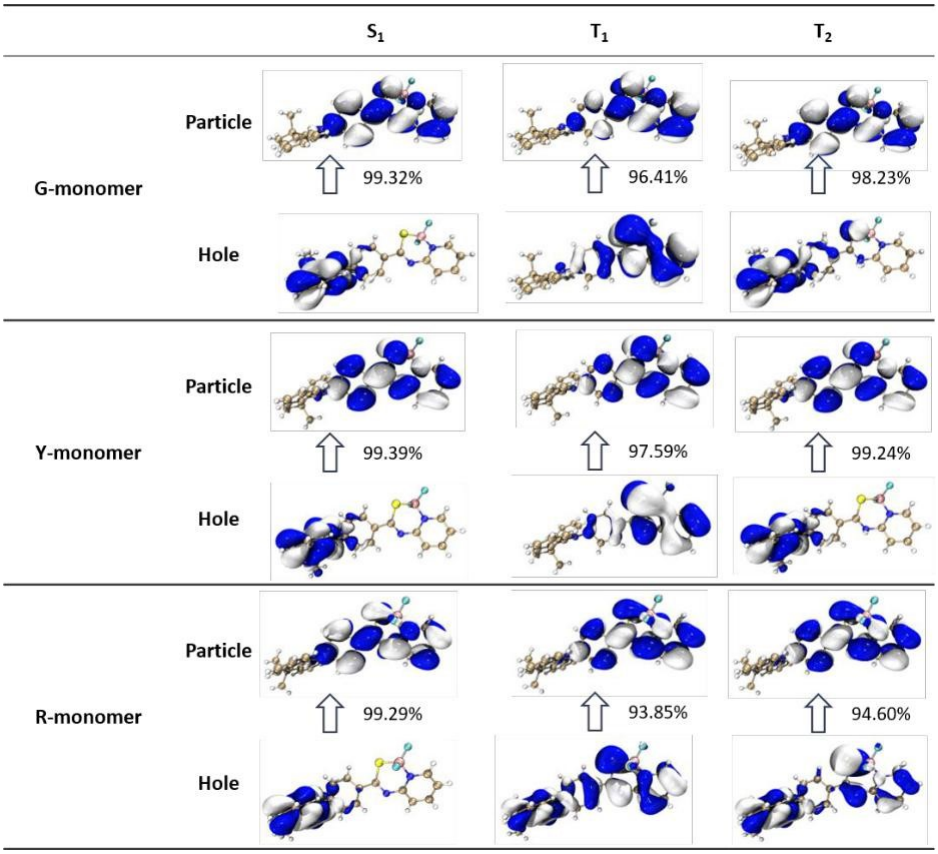

Figure S10. NTO analysis of S_1, T_1 and T_2 for monomers in G-Crystal, Y-Crystal and R-Crystal.

Table S3. Energy levels of monomers in G-, Y- and R-Crystal

	S_1 (eV)	T_1 (eV)	T_2 (eV)	T_3 (eV)
G-monomer	3.14	2.97	3.10	3.48
Y-monomer	3.25	3.00	3.24	3.51
R-monomer	3.08	3.00	3.06	3.54

Table S4. SOC constants of monomers in G-, Y- and R-Crystal

	$\xi(S_0\text{-}T_1)$ (cm^{-1})	$\xi(S_1\text{-}T_1)$ (cm^{-1})	$\xi(S_1\text{-}T_2)$ (cm^{-1})
G-monomer	6.27	3.33	1.23
Y-monomer	6.23	3.57	0.25
R-monomer	6.25	2.49	2.33

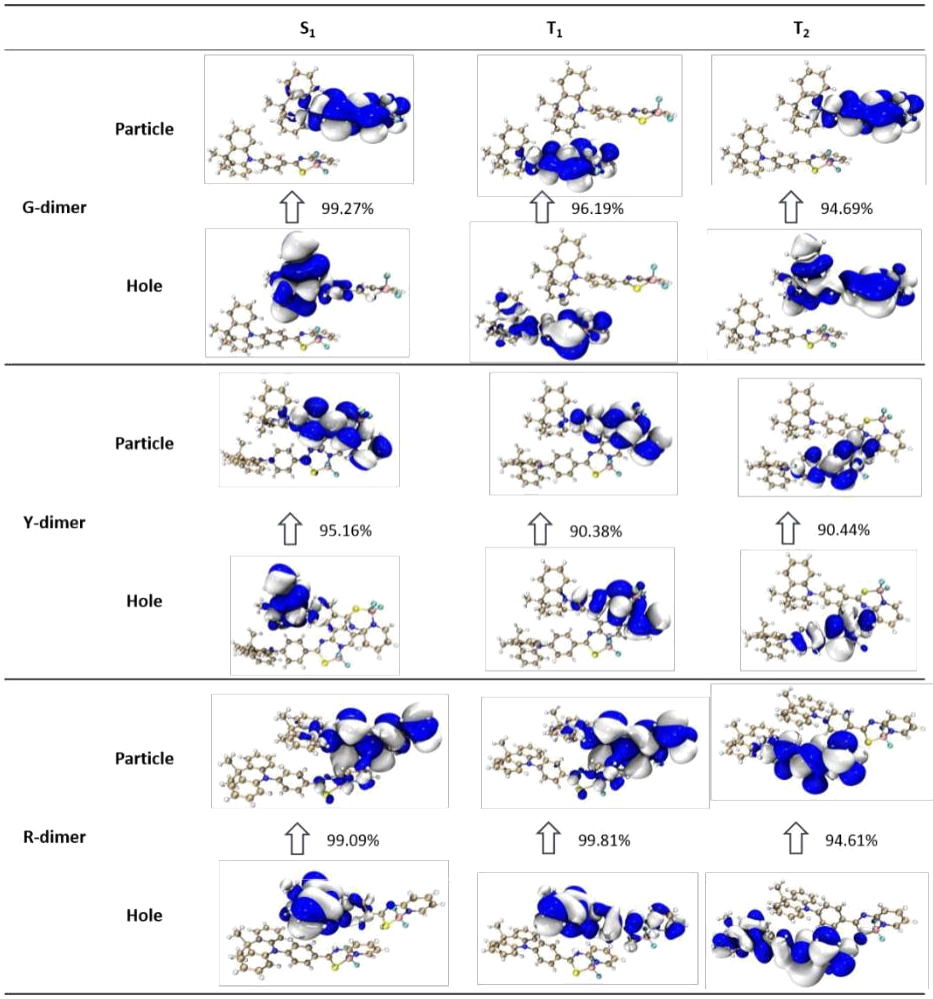

Figure S11. NTO analysis of S_1, T_1 and T_2 for dimers in G-Crystal, Y-Crystal and R-Crystal.

Table S5. Energy levels of dimers in G-, Y- and R-Crystal

	S_1 (eV)	T_1 (eV)	T_2 (eV)	T_3 (eV)
G-dimer	2.99	2.94	2.96	3.01
Y-dimer	3.25	3.00	3.01	3.24
R-dimer	2.94	2.90	3.01	3.04

Table S6. SOC constants of dimers in G-, Y- and R-Crystal

	$\xi(S_0\text{-}T_1)$ (cm^{-1})	$\xi(S_1\text{-}T_1)$ (cm^{-1})	$\xi(S_1\text{-}T_2)$ (cm^{-1})	$\xi(S_1\text{-}T_3)$ (cm^{-1})
G-dimer	6.81	2.02	2.48	2.43
Y-dimer	6.86	3.01	1.05	0.20
R-dimer	5.18	0.83	0.44	2.84

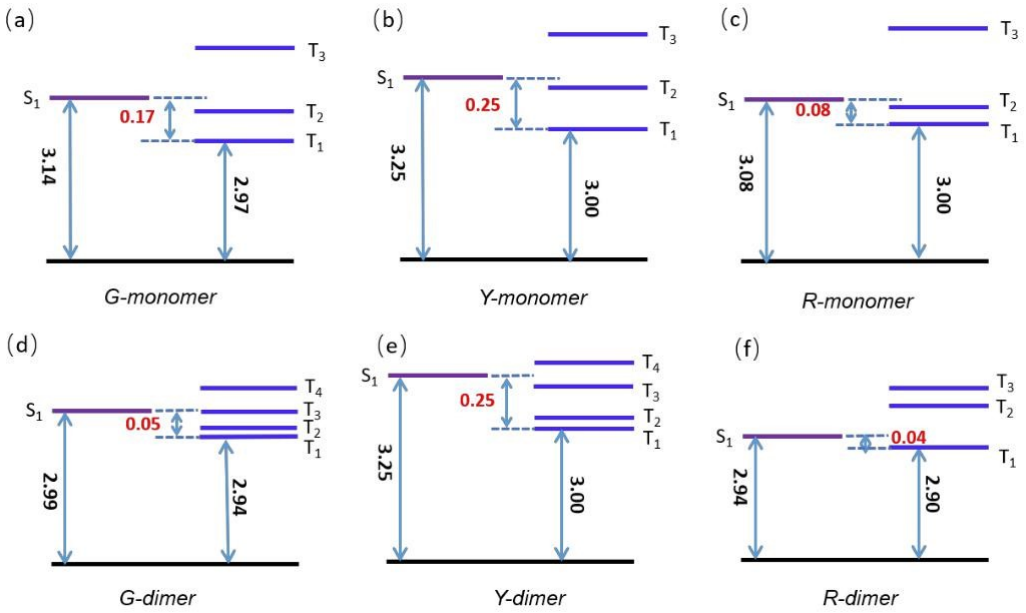

Figure S12. TD-DFT calculated energy level diagram of monomers and dimers in G-Crystal, Y-Crystal and R-Crystal.

5.2. The calculation results of different conformations in G-Crystal:

The above data of G-monomer are calculated from G1 conformation. We compared the calculation data of G1 and G2 conformation in the following.

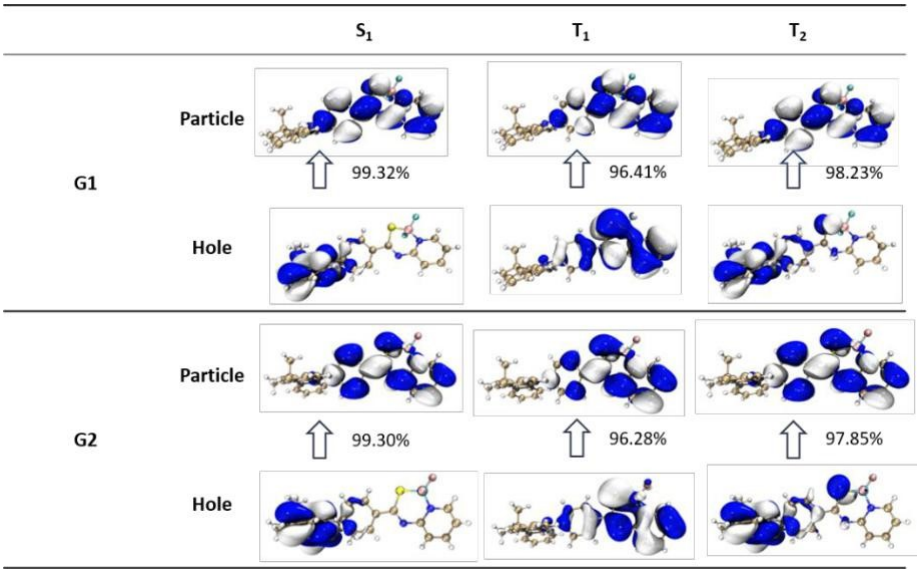

Figure S13. NTO analysis of S_1, T_1 and T_2 for G1 and G2.

Table S7. Energy levels of conformations of G1 and G2

	S_1 (eV)	T_1 (eV)	T_2 (eV)	T_3 (eV)
G1	3.14	2.97	3.10	3.48
G2	3.16	2.98	3.13	3.50

Table S8. SOC constants of conformations of G1 and G2

	$\xi(S_0\text{-}T_1)$ (cm^{-1})	$\xi(S_1\text{-}T_1)$ (cm^{-1})	$\xi(S_1\text{-}T_2)$ (cm^{-1})
G1	6.27	3.33	1.23
G2	6.83	3.45	1.48

As we can see, the calculation results of G1 and G2 are similar to each other. So the different conformations of G1 and G2 have little impact on the whole photophysical properties of G-Crystal.

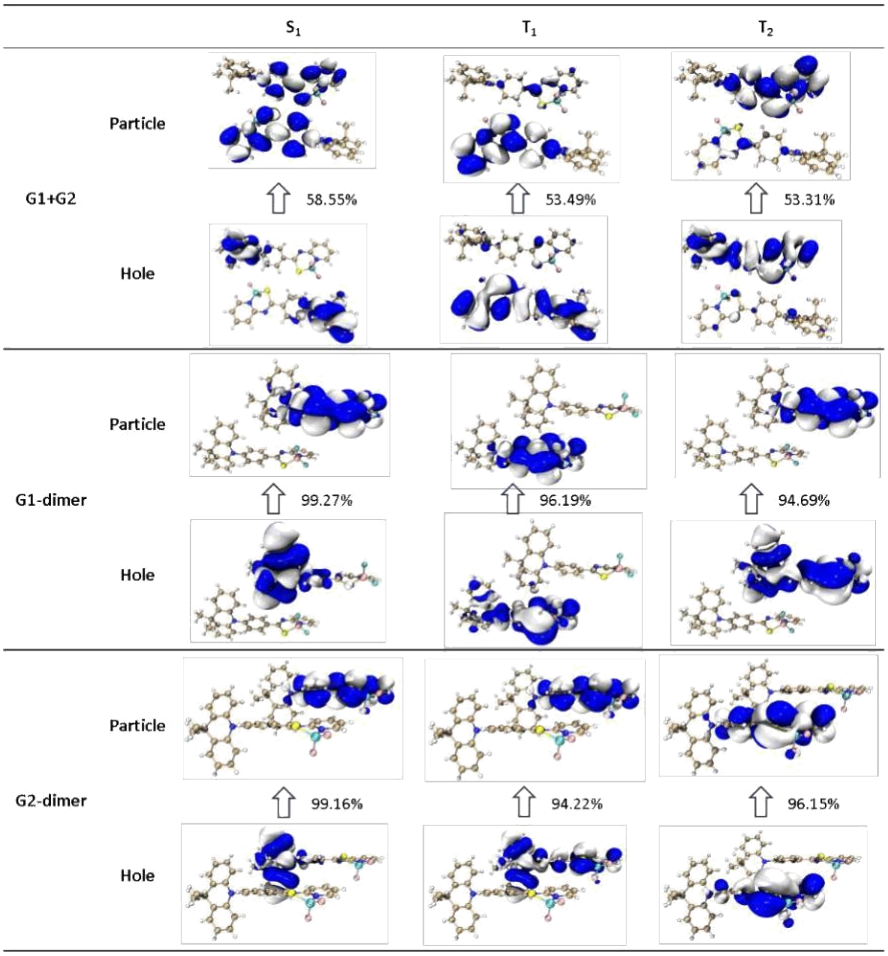

Figure S14. NTO analysis of S1, T1 and T2 for different dimers in G-Crystal.

Table S9. Energy levels of different dimers in G-Crystal

	S_1 (eV)	T_1 (eV)	T_2 (eV)	T_3 (eV)
G1-dimer	2.99	2.94	2.96	3.01
G2-dimer	2.99	2.93	2.95	3.00
G1+G2	3.05	2.96	2.97	3.04

Table S10. SOC constants of different dimers in G-Crystal

	$\xi(S_0\text{-}T_1)$ (cm^{-1})	$\xi(S_1\text{-}T_1)$ (cm^{-1})	$\xi(S_1\text{-}T_2)$ (cm^{-1})	$\xi(S_1\text{-}T_3)$ (cm^{-1})
G1-dimer	6.81	2.02	2.48	2.43
G2-dimer	6.80	2.05	0.08	2.43
G1+G2	9.70	2.44	0.23	0.63

The calculation results (energy levels and SOC constants) of G1-dimer and G2-dimer are almost the same. Furthermore, the hole-particle distributions of G1-dimer and G2-dimer are quite similar, and they all derive from a single monomer. For G1+G2, its S_1 and T_1 energy levels are obviously higher than those of G1-dimer and G2-dimer, which does not support the existence of the excimer. These results indicate that the property of G-Crystal should be dominant by the monomer unit.

6. Thermal analysis and hot stage microscopy (HSM) studies

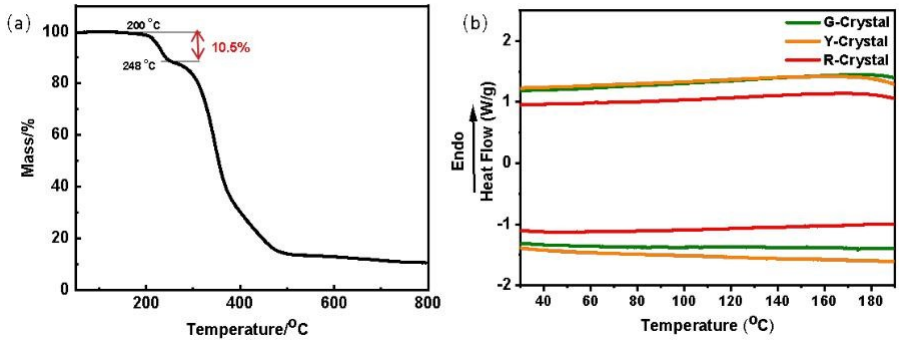

Figure S15. TGA profiles of DMAC-PSBF2 (a). DSC profiles of the G-, Y- and R-Crystal (b).

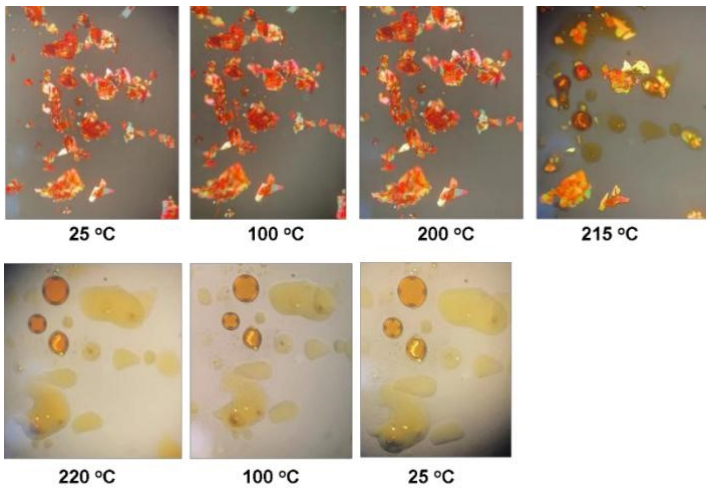

Figure S16. Photomicrographs of R-Crystal captured during 25-220 ^{O}C over HSM studies.

The TGA studies show that when temperature raised to 200 ^{O}C, the weight loss reached to 1%. Continued heating further showed a 10.5% weight loss until 248 ^{O}C, which agrees well with the first peak in DTG curve. The 10.5% weight loss indicates that the molecule DMAC-PSBF2 ($C_{27}H_{22}BF_2N_3S$, 469.2 g/mol) probably lossed BF_2 (49.0 g/mol) unit. DSC studies showed a smooth curve during the heating and cooling processes, which suggest that there has no polymorphic phase transition. We could not found any transformation through HSM studies either (Figure S15). Before heating to 200 ^{O}C, the R-Crystal remained constant. When the temperature turned to 215 ^{O}C, it tended to melt. But according to the TGA, the molecule started to decompose when the temperature level exceeded 200 ^{O}C. The red crystal turned to orange when cooling from 220 ^{O}C. We arribute the color-changing phenomenon to thermolysis.

7. NMR spectra

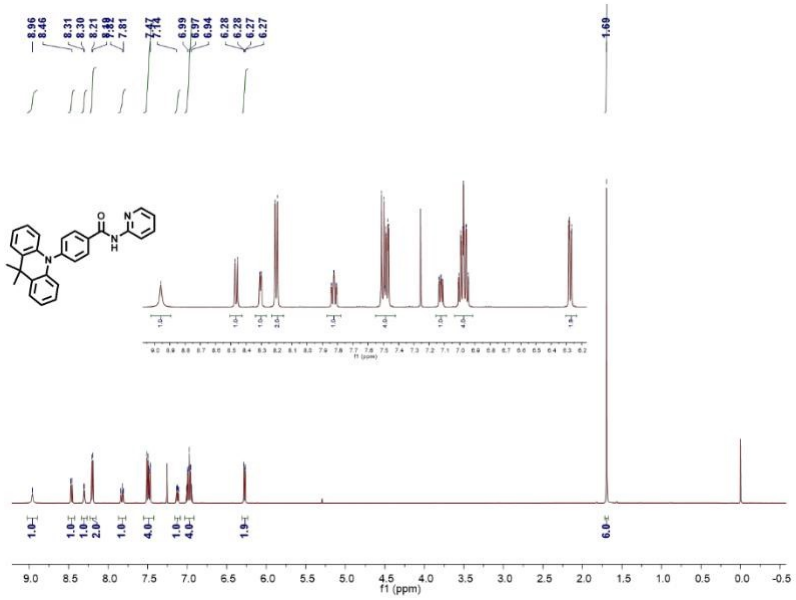

Figure S17. ^{1}H NMR of DMAC-PA.

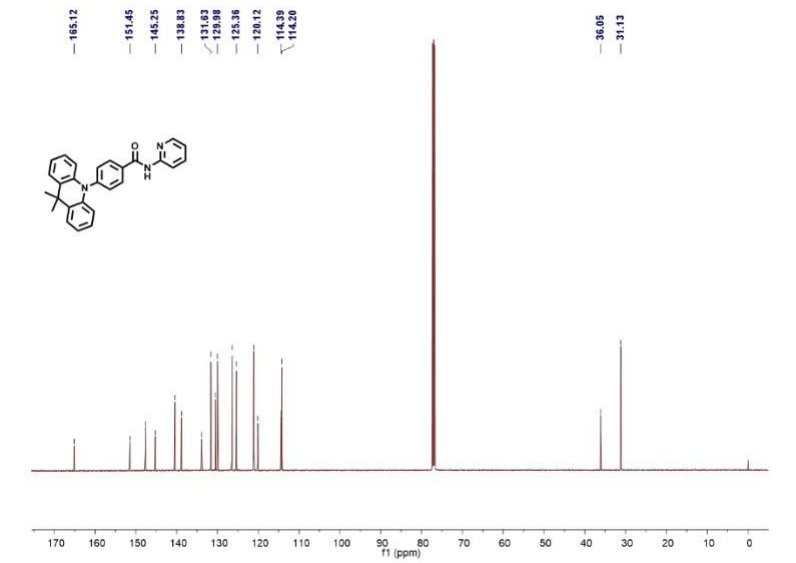

Figure S18. ^{13}C NMR of DMAC-PA.

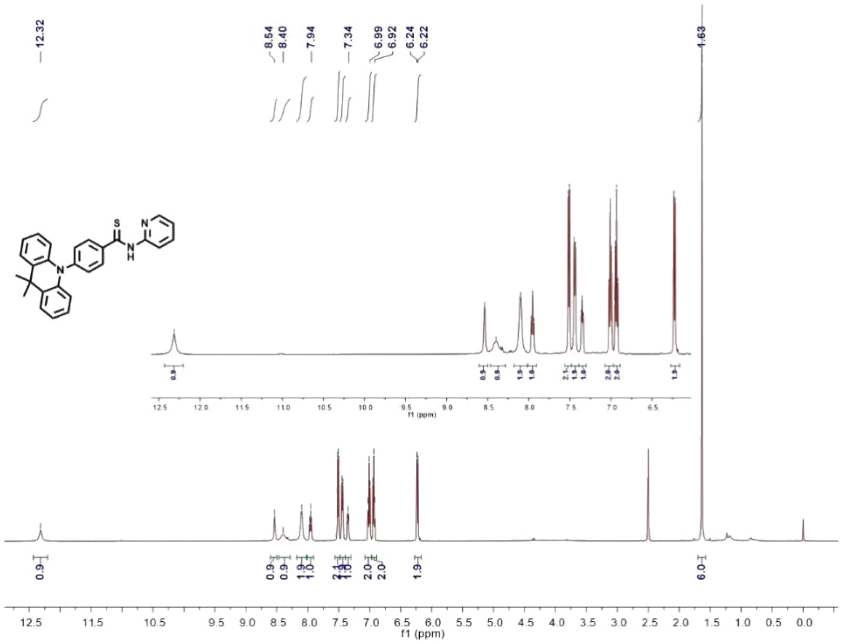

Figure S19. ^{1}H NMR of DMAC-PS.

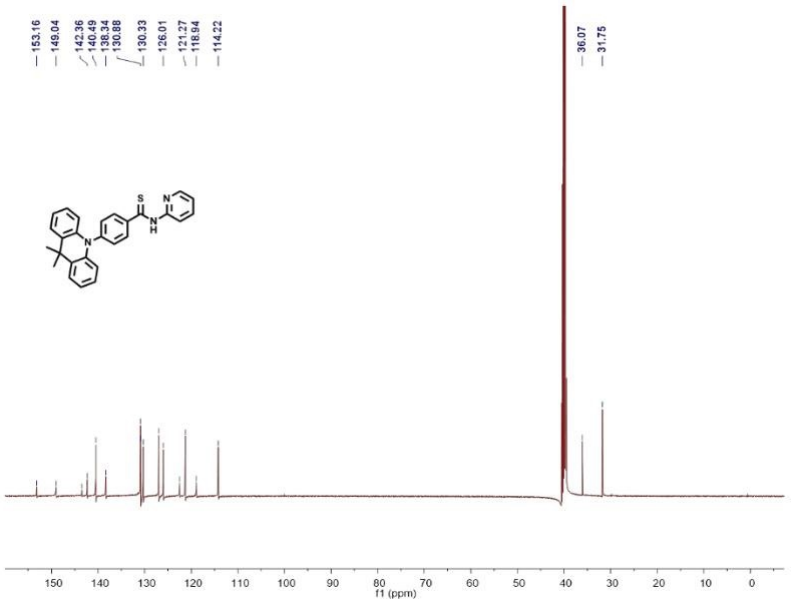

Figure S20. ^{13}C NMR of DMAC-PS.

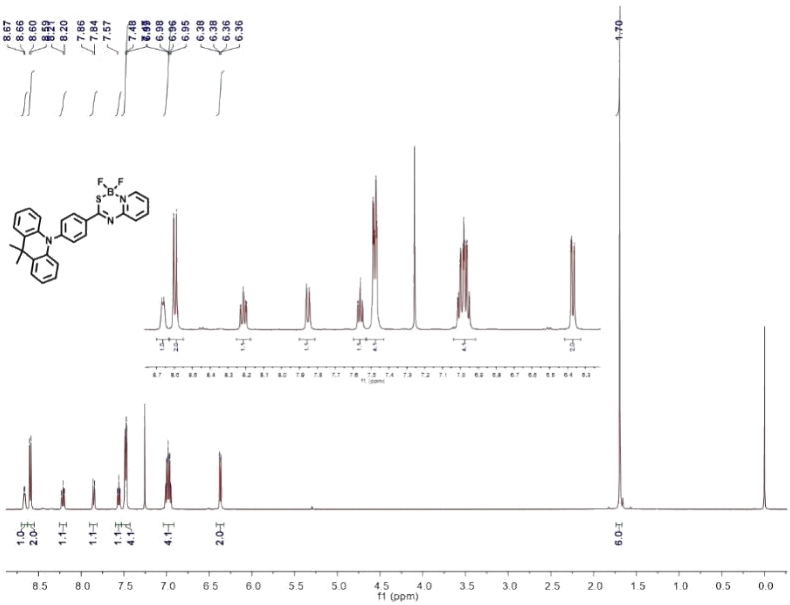

Figure S21. ^{1}H NMR of DMAC-PSBF2.

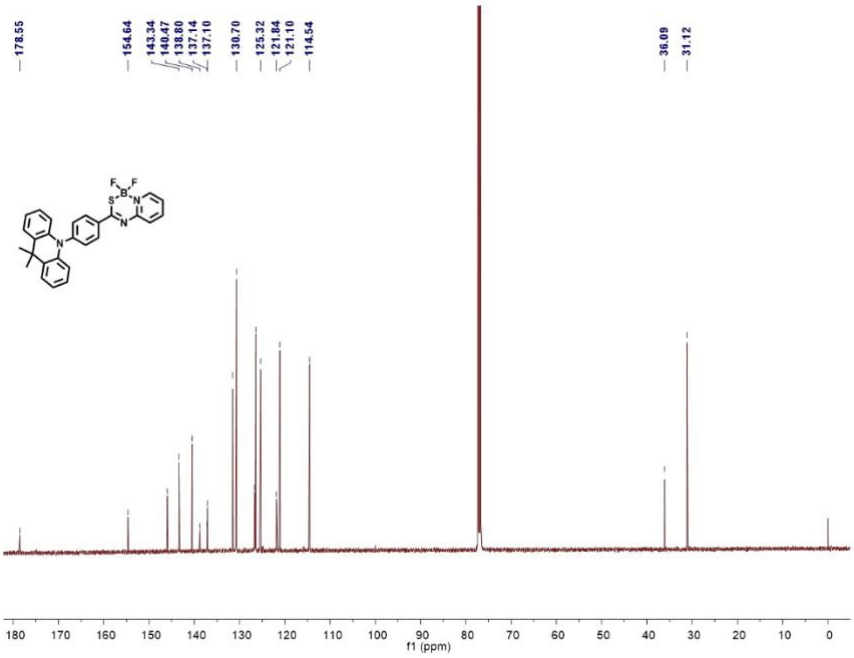

Figure S22. ^{13}C NMR of DMAC-PSBF2.

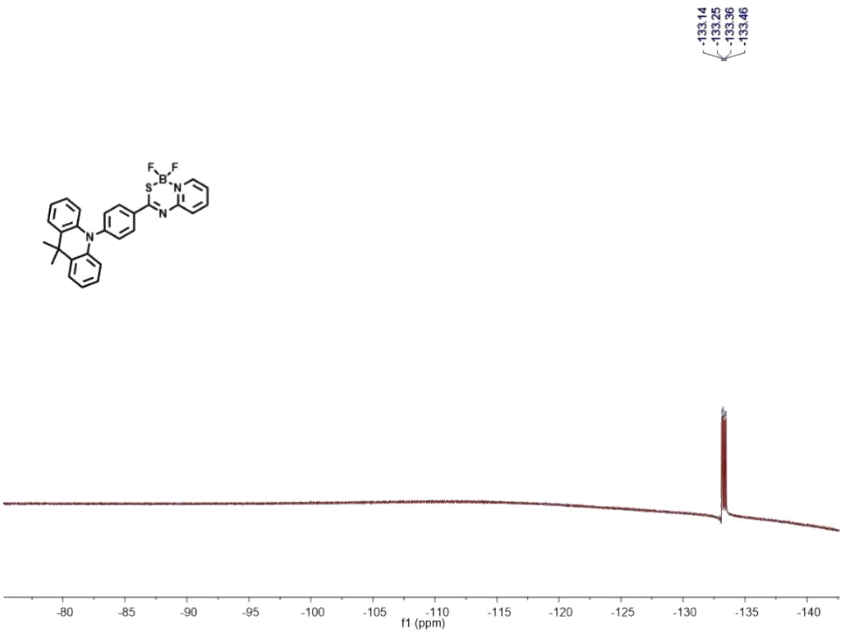

Figure S23. ^{19}F NMR of DMAC-PSBF2.

8. References

[1] S. Yang, H. Yan, X. Ren, X. Shi, J. Li, Y. Wang, G. Huang, *Tetrahedron*. 2013, **69**, 6431-6435.

[2] T. Lu, F. Chen, *J. Comput. Chem.* 2012, **33**, 580-592.

[3] F. Neese, *WIREs. Comput. Mol. Sci.* 2018, **8**, e1327.